Colloids and Surfaces A: Physicochemical and Engineering Aspects 670 (2023) 131583

Contents lists available at ScienceDirect

Colloids and Surfaces A: Physicochemical and Engineering Aspects

journal homepage: www.elsevier.com/locate/colsurfa

Coarse-grain molecular dynamics simulation framework to unravel the interactions of surfactants on silica surfaces for oil recovery

Germán Pérez-Sánchez [a,*], Filipa M. Costa [a], Gonçalo M.C. Silva [a], Manuel M. Piñeiro [b], João A. P. Coutinho [a]

[a] CICECO – Aveiro Institute of Materials, Department of Chemistry, University of Aveiro, 3810-1933 Aveiro, Portugal
[b] CINBIO, Department of Applied Physics, University of Vigo, 36310, Spain

GRAPHICAL ABSTRACT

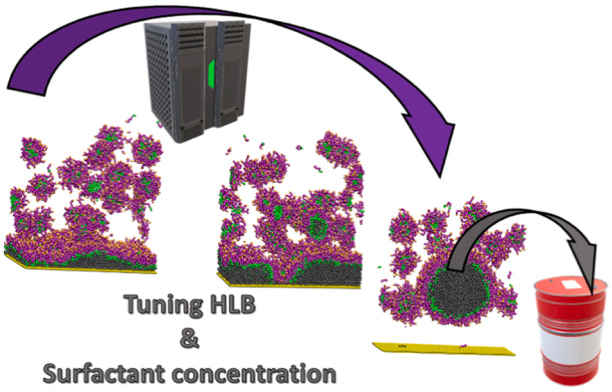

ARTICLE INFO

Keywords:
MARTINI coarse-grain model
Surface oil removal
Molecular dynamics
Surfactant aqueous solutions

ABSTRACT

A coarse-grained molecular dynamics (CG-MD) framework, based on the MARTINI 3.0 model, was developed to characterise the interactions between surfactants and oil-silica substrates to resemble chemical enhanced oil recovery (EOR) processes. Previous computational studies, at the atomistic scale, addressed interactions between surfactants and oil over diverse surfaces. Even though simulations provided significant information involved throughout different stages of oil extraction from surfaces, atomistic scale simulations fail when approaching the time and size scale required to address the surfactant phase behaviour that can also impact the oil detachment. Our coarse-grained model aims to overcome the lack of computer approaches that can tackle the surfactant self-assembly and the formation of ordered structures in the removal of oil from silica substrates. A new MARTINI 3.0 coarse-grain framework to model silica surfaces and aqueous solutions of C_iE_j and C_{16}TAB surfactants is presented. Coarse-grained simulations entailing a silica surface, covered by dodecane or eicosane were brought in contact with aqueous solutions of C_{16}TAB and four nonionic C_iE_j (C_8E_6, C_8E_{12}, $C_{12}E_6$, $C_{16}E_{12}$) surfactants to resemble EOR processes with a size/time scale several orders of magnitude larger than previous simulations. The impact of concentration and hydrophilic-lipophilic balance (HLB) of surfactants on the detachment of dodecane and eicosane from the silica surface was evaluated by visual inspection of the simulation snapshots and the

* Correspondence to: Aveiro Institute of Materials, Department of Chemistry, University of Aveiro, Spain.
E-mail address: gperez@ua.pt (G. Pérez-Sánchez).

https://doi.org/10.1016/j.colsurfa.2023.131583
Received 3 March 2023; Received in revised form 30 April 2023; Accepted 1 May 2023
Available online 2 May 2023

evolution of the solvent accessible surface areas (SASA). In contrast with previous atomistic simulations, nonionic surfactants seem the best candidates for an optimal oil removal from silica-based surfaces whereas the presence of charged moieties hinders the process. Diluted nonionic CE aqueous solutions were shown to be the most effective solutions, unlike more concentrated ones. When compared with dodecane, eicosane was less prone to be removed from the silica surface due to the increased alkyl chain length. Our study demonstrates that not only the surfactant nature but also the phase behaviour, clearly impact the detachment of oil from silica surfaces. This is an important aspect to consider for a proper choice of surfactants in EOR processes, that is only attainable through a coarse-grained framework.

1. Introduction

Despite the depletion of natural reservoirs, oil and gas remain our predominant source for energy and raw materials [1]. Oil extraction processes commonly encompass two phases: in a first stage, the oil is recovered through a natural flow, or an artificial lift process, followed by a second step consisting of gas injection and/or waterflooding. However, two-thirds of the initial oil remain in the reservoir. This oil can be retrieved by specialized chemical processes known as Enhanced Oil Recovery (EOR) [2–4]. EOR processes use different techniques [5,6] usually divided into three main types: thermal, chemical and gas injection [7]. In chemical EOR, aqueous solutions of surfactants [8] are injected into the reservoir to reduce the water-oil interfacial tension (IFT), [9] aiding the oil detachment from reservoir rock surfaces. Depending on the conditions, the surfactants can self-assemble into different structures that may promote or prevent the solubility of the oil towards the aqueous phase [10]. Many experimental studies addressed important aspects of chemical EOR aiming the phase behaviour, [11] water/oil interfacial tensions (IFT), [12] substrate wettability, [13] or foaming ability, [14] demonstrating the role of surfactants on decreasing the water/oil IFT to separate the oil from the surface of reservoir rocks [15]. However, the diversity of components of crude oil and macroscale structural factors complicate the understanding of the molecular mechanisms behind detachment of oil. Theoretical studies are vital to unveil molecule scale interactions between surfactants, oil, and surfaces. All-atom molecular dynamics (AA-MD) simulations can provide significant insight in the oil/water and oil/water/surfactant interfacial interactions. [15-26], AA-MD studies argued that the oil detachment from silica surfaces can be summarised in three main stages; an initial formation of water channels, as observed in experiments, [20] perpendicular to the oil-silica substrate upon surfactant addition. Afterwards, the first layer of oil attached to the surface is disrupted due to the strong electrostatic interactions between water and silica. In the final stage, the oil form droplets that detach the silica surface through buoyancy forces [15,17]. Bearing this in mind, Tang et al. [15] developed a detailed AA-MD study to analyse these stages by attempting different polarities for the silica surface and using diverse nature ionic and nonionic surfactants. The aim was to unveil the mechanisms behind the formation of water channels and the final disruption of the oil layer attached to the silica surface. They demonstrated that surfactant-oil interactions, its flow speed, and the polarity of the silica surface drive the formation of water channels throughout the oil layer. However, their AA-MD simulations were limited to small samples ($\sim 6 \times 6 \times 6$ Å) with few surfactants (20) and simulated by a relatively short period of simulation time (40 ns). At this scale, the impact of surfactant self-assembly such as the formation of micelles or long-range ordered phases, that can impact the oil detachment, cannot be naturally captured.

CG-MD models can bridge the gap between AA-MD simulations and the real conditions that can be found in natural oil reservoirs whilst reconciling conflicting observations [21,22]. In fact, Tang et al. [15] argued that AA-MD models cannot tackle mesoscale structural features of silica surfaces such as pores and defects and their influence in oil detachment. Unfortunately, few CG-MD simulation studies addressed interactions between aqueous solutions of surfactants and oil attached to surfaces. Katiyar et al. [23] analysed the interactions between silica nanoparticles and nonionic surfactants at the water-oil interface using CG-MD MARTINI 2.2 simulations. In this work, the authors showed that the interfacial tension, at the silica nanoparticle-oil interface, depends on the tendency of the nonionic surfactants to be adsorbed besides the concentration of both, silica nanoparticles, and surfactants. The study stated that the formation of hydrogen bonds drives the adsorption where the pH has an important impact as shown in experiments. However, this scenario is not representative of EOR processes, as the geometry of the silica nanoparticles does not resemble a silica surface, which can have significant impact on the attachment/detachment mechanism of oil. Thereby, a CG-MD simulation platform to tackle the impact of surfactant self-assembly and phase behaviour in the detachment of oil from silica surfaces is still missing. For this purpose, we aimed the development of a CG-MD simulation framework to analyse, at the proper time and size scale, the interactions of aqueous solutions of surfactants in oil-silica substrates. Two surfactants were selected, the cationic C_{16}TAB and nonionic polyether-based surfactants since they are of special interest in chemical EOR due to their high boiling point, hygroscopicity, non-corrosiveness, freezing point depression and lubrication properties, as well as their ability to act as freezing point depressants and hydrate inhibitors.[24] Poly(oxyethylene) alkyl ethers are a particular case of nonionic surfactants with the general chemical formula $H(CH_2)_i(OCH_2CH_2)_jOH$, also denoted as C_iE_j, where *i* corresponds to the number of carbons in the hydrophobic tail and *j* is the number of ethylene oxide groups (EO). The relatively low environmental impact due to their biodegradability, ease of synthesis, stability in high salinity media, and the favourable cost/efficiency ratio of C_iE_j surfactants make them one of the best choices for EOR processes [25–27]. Moreover, with the possibility of tailoring the length of the hydrophobic and hydrophilic chains, it is possible to tune their hydrophilic-lipophilic balance (HLB) [16–18], [28] A good understanding on how the surfactant concentration impacts the oil detachment is crucial to design and prepare solutions for EOR processes [29]. Thus, a reliable computer model that can capture the entire phase behaviour, at different concentrations, for selected aqueous solutions of surfactants is vital to construct a proper CG-MD simulation framework to tackle EOR processes. Upon self-assembly, C_iE_j can display diverse morphologies, ranging from spherical or worm-like micelles under diluted conditions to more complex hexagonal, gyroid or bilayer phases at higher concentrations [30–32]. When considering the type of surfactant, the formation of highly viscous liquid crystal (LC) or gel-like phases must be considered [33]. Different experimental techniques such as Small-Angle X-Ray scattering (SAXS), Small-Angle Neutron Scattering (SANS), and Polarizing Optical Microscopy (POM) have been used to characterize micellar regimes [34,35] and diverse mesophases found at higher concentrations [36,37]. However, some approximations and/or limitations inherent to the experimental techniques have yielded conflicting results. For instance, the phase diagram of $C_{10}E_5/H_2O$ reported by Nibu and Inoue [38] shows the existence of a bi-continuous cubic phase (V_1) in the concentration range between the lamellar (L_α) and hexagonal (H_1) phases whereas Lang and Morgan, [39] using a different experimental technique, reported only L_α and H_1 phases. Similar conflicting results depending on the experimental setup can be found in the literature for $C_{10}E_6$, [38,40,41] $C_{12}E_2$, [42,43] $C_{12}E_6$ [36,44] and $C_{12}E_8$ [36,45–47].

AA-MD simulation tackling diverse C_iE_j aqueous solutions tried to shed light into this issue but they were limited to the initial stages of self-assembly [29,48–54]. CG-MD models reduce the computational demand by grouping atoms with similar physico-chemical characteristics as single interaction centres, reducing the computational cost, and opening the door to access the entire phase behaviour.[21,55] The first CG-MD attempt to model C_iE_j surfactants was reported by Shinoda et al. [56] where the non-bonded parameters were developed using experimental density, surface tension and hydration free energies data whereas bonded parameters were fitted to match AA-MD simulations. The lack of hydration free energies to fit the EO-water interaction parameters was circumvented with values of lamellar spacing and molecular area from the L_α phase of an aqueous solution of $C_{12}E_2$. Later, the same authors [57] developed a CG-MD model for aqueous solutions of $C_{12}E_6$ where the predicted hexagonal, H_1, and lamellar, L_α, phases were in good agreement with experiments [36,44]. Even though other CG-MD approaches can be found in the literature tackling C_iE_j surfactants, [58–62] most of them rely on MARTINI 2.2 [55]. Initially developed for phospholipid biomolecular systems, it promptly was extended to a wide variety of organic and inorganic compounds [63,64]. MARTINI 2.2 has been widely adopted due to its simplicity since the non-bonded interactions are included as pre-defined bead types, whose interactions are summarized in a very simple energy matrix of interactions (four main bead types). Throughout this matrix of interactions, which was parameterized to match densities, self-diffusion constants, and partitioning free-energies of representative organic compounds, [55] a wide number of molecules can be CG-mapped. However, the pre-defined MARTINI 2.2 beads for EO groups seem too hydrophilic, [61,63] yielding erroneous results for C_iE_j surfactants in non-polar media. Grunewald et al. [65] developed an ad hoc MARTINI 2.2 bead for EO groups which successfully reproduced the experimental density of PEO and captured the structure of lipid bilayers as well as the phase behaviour of some C_iE_j surfactants. Recently, this model was benchmarked to a wide number of C_iE_j surfactants by Crespo et al. [30] since previous attempts [61] only addressed a restricted concentration range of $C_{12}E_2$, $C_{12}E_4$, and $C_{12}E_6$. Crespo et al. [30] evaluated the impact of the hydrophobic and hydrophilic tail lengths over a wide range of HLB and surfactant concentrations to reproduce the entire phase behaviour of aqueous solutions of C_iE_j surfactants, an important aspect when using them as surfactants in chemical EOR. The C_{16}TAB was widely studied through different computer scales, successfully exploring the phase behaviour, and the CG-MD model was taken from the literature [21,22,66].

Our work aims to cope the lack of CG-MD models that can resemble EOR processes at the time/size scale necessary to evaluate the impact of the surfactant phase behaviour in the detachment of oil from silica surfaces. Throughout the development of our CG-MD framework, we revealed some limitations of MARTINI 2.2 to model silica-water interfaces and the necessity of the improved MARTINI 3.0 [67] to model silica surfaces, C_iE_j and C_{16}TAB surfactants in aqueous solutions. A careful validation process, detailed in the supplementary material section, was followed based on experimental and theoretical micellar size distributions of C_iE_j and C_{16}TAB surfactants. Remarkably, the results overcome some of the limitations noticed in the phase behaviour characterisation of C_iE_j aqueous solutions reported by Crespo et al. [30] based on MARTINI 2.2. With the new CG-MD MARTINI 3.0 framework, the impact of concentration and HLB of the above surfactants in the detachment of dodecane and eicosane from a silica surface was evaluated. Our CG-MD framework increases the size and time scale of previous AA-MD simulations by several orders of magnitude, closing the gap between the atomistic scenario and the macroscopic scale involved in EOR processes, allowing the natural surfactant self-assembly above oil-silica substrates.

2. Methodology

2.1. Simulation details

Classical MD simulations were performed with GROMACS 2021 [68] and the leapfrog algorithm [69] to integrate the equations of motion with a 10 fs of time step. Non-bonded interactions included the Lennard-Jones (LJ) potential and the Coulombic term with the potential-shift-verlet modifier in both and a cut-off radius of 1.1 nm. The long-range electrostatic interactions were calculated with the Particle-Mesh-Ewald (PME) [70]. The temperature was fixed to 298 K using the velocity-rescaling thermostat [71] with a coupling time constant of $\tau_T = 1.0$ ps. Initially, the MARTINI 2.2 based topology for C_iE_j surfactants was taken from Grunewald et al. [65] where bonded interactions included bond stretching and angle bending. The harmonic potential of the bond stretching was constrained with the LINear Constraint Solver (LINCS) [72]. The angle bending included a restricted potential developed by Bulacu and co-workers [73] to stabilize the bond angle when approaches 180º and dihedrals were also included as described in Grunewald et al. [65] The CG models for C_{16}TAB surfactant, water and the oil samples were taken from MARTINI 2.2 [55]. The MARTINI 2.2 CG model for silanol developed by Perrin et al. [74] was selected to build our rigid silica-based surface. The CG mapping scheme for the above systems is described in Appendix A1 of the supplementary material section.

Packmol [75] was used to build the initial rectangular shape of the simulation boxes with periodic boundary conditions in all directions. Each compound, (oil, surfactant, and water) was arranged as layers in the normal direction to the plane delimited by the silica surface. Simulations were visualized using the Visual Molecular Dynamics (VMD) software package, [76] and the micellar distributions were investigated using an in-house code [21] which implements the Hoshen-Kopelman cluster-counting algorithm [77]. This algorithm considers that two surfactants belong to the same aggregate when neighbour surfactants end tails are separated by less than 1.6 nm, which corresponds to the first minimum of the respective radial distribution functions. Number density profiles and solvent accessible surface areas (SASA) were obtained with the *gmx density* and the *gmx sasa* GROMACS tools, respectively.

2.2. Molecular modelling and coarse-grained model validation

MARTINI 3.0 [67] brought a larger parameter set and additional interaction modifiers which should yield higher flexibility. The release of a more realistic water model, including three mapping options; W, SW, and TW for 4, 3 and 2 implicit water molecules, respectively, aims to address the shortcomings of the previous model (details in Appendix A2 of the supplementary material section). In addition to the previous polar (P), intermediately polar (N), apolar (C) and charged (Q) bead types, a new D bead was included for divalent ions besides a X bead to reproduce halogen-based groups. New interactions modifiers (still denoted as subscripts) for all bead types were included such as the *q* subscript to incorporate partial charges (only whole charges were possible in MARTINI 2.2), the *h* and *r* self-interaction modifiers to capture the impact of dispersive interactions, mimic dipole moments or reduce/increase miscibility with other particles. Furthermore, chemically specific modifiers for P an N bead types are still available such as *d* and *a* for donor or acceptor hydrogen-bonding capabilities, respectively. The *v* and *e* subscripts denote electron rich or poor, respectively, to emulate electron polarizabilities. Furthermore, *p* or *n* subscripts denoting electron donor and acceptor, respectively, were developed to replicate the Hofmeister series of monovalent and divalent ions. Additionally, MARTINI 3.0 now includes cross interaction terms that were missing in the previous MARTINI 2.2. The favourable perspectives of MARTINI 3.0 suggest that the issues found in MARTINI 2.2 with the unrealistic freezing of water could be surpassed (Figure A2.2b in Appendix A2 of

the supplementary material section). This encouraged us to extend the MARTINI 2.2 parameters for the silica surface as well as the surfactants to the new MARTINI 3.0. The model for dodecane and eicosane in MARTINI 3.0 remains the same as in MARTINI 2.2, involving C_1 apolar beads. For the silica surface, the N_d bead (MARTINI 2.2) was replaced by the SN_{1dq} bead since it encompasses similar interactions energies. A validation process was carried out by reproducing the dodecane layer of 1664 molecules arranged over the silica surface. Under the new parameterisation, the density profile of the dodecane was in very good agreement with the previous MARTINI 2.2 results and the literature data [15], as illustrated in Appendix A2 (Figure A2.1a) in the supplementary material section.

The parameterisation of C_iE_j and $C_{16}TAB$ surfactants consisted of finding analogous interaction energies (used in MARTINI 2.2) to the new MARTINI 3.0. Our choice for the water model was the TW (2:1 mapping) since it guarantees a much better energy landscape [67]. The validation process focused on diluted solutions to compare their micelle size distributions with the previous MARTINI 2.2 results and experimental data. Four surfactants C_8E_6, $C_{12}E_6$, $C_{16}E_{12}$ and $C_{16}TAB$, encompassing three nonionic and one ionic surfactant with diverse amphiphilic characters, were selected. The equivalent MARTINI 3.0 beads for C_iE_j were SN_{3q} (ethylene oxide groups), SP_6 (terminal C_2OH group) and SC_{1h} beads (alkyl tail), were chosen to substitute EO, SP_2, and C_1 beads, respectively. In the new model a 3:1 mapping was selected since it reproduces the diverse EO and alkyl tail lengths of the C_iE_j family. The q subscript in SN_{3q} represents an increase in self-interactions besides with water when compared with the MARTINI 2.2 SN_3 bead. The subscript h in SC_{1h} introduces small differences in dispersive interactions and reduces miscibility with non-labelled beads [67]. The parameters for the $C_{16}TAB$ surfactant were taken from Souza et al.[67] suggesting a Q_2 bead for tetra butyl ammonium groups whereas C_1 beads map the alkyl tail as in the previous model. In MARTINI 3.0 bromide counterions are represented by SQ_4 bead type.

A set of CG-MD simulations with surfactant concentrations above their critical micelle concentrations, 13% wt. for the nonionic C_8E_6 the $C_{12}E_6$ and $C_{16}E_{12}$ surfactants and 6%wt. for the cationic $C_{16}TAB$, were run along 1000 ns of simulation time. The micelle size distributions obtained in the simulations are displayed in Table 1.

Table 1 reveals a good match between the selected MARTINI 3.0 parameterisation and experimental data, improving the previous MARTINI 2.2 results. Thus, MARTINI 3.0 parameterisation used for C_iE_j and $C_{16}TAB$ surfactants besides the silanol groups, dodecane, eicosane and the TW water molecules are summarised in Fig. 1.

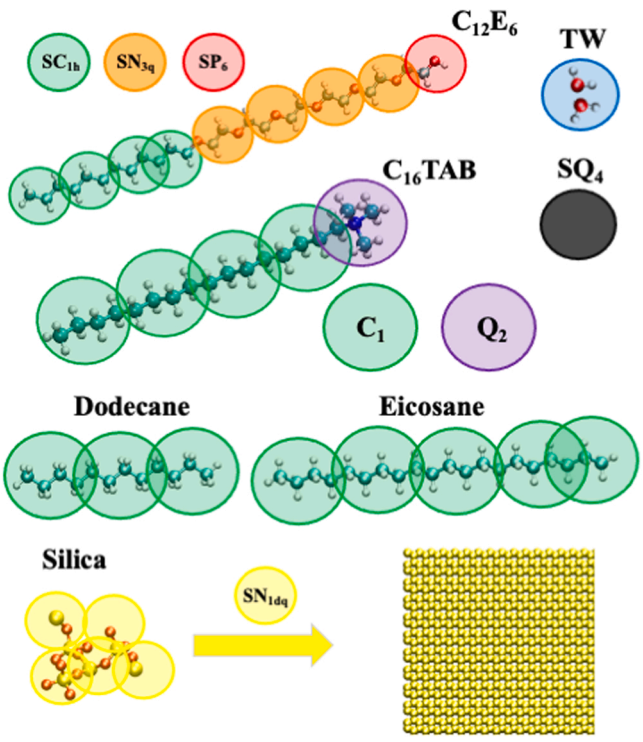

Fig. 1. MARTINI 3.0 mapping scheme for the systems used in this study. The $C_{12}E_6$ surfactant is shown as an example of how the C_iE_j moieties are configurated. "S" labelled beads involve three no-hydrogen atoms (3:1 mapping) whereas regular beads include four (4:1 mapping). The coarse-grained beads are represented by coloured circles with green and red colour symbolising apolar and polar characters, yellow and orange different strengths of non-polar beads (intermediate character between polar and apolar). The ammonium charged bead is denoted in purple, bromide counterions in black and the TW water (2:1 mapping) in blue. An illustration of the silica surface is shown on the bottom right.

3. Results and discussion

3.1. CG-MD simulation snapshots analysis

Four nonionic C_iE_j surfactants entailing different alkyl tail lengths and EO groups were selected to assess the impact of the hydrophilic-lipophilic balances in the detachment of model oils (dodecane or eicosane) from a silica surface. Details about the simulation box sizes and number of components used in the simulation runs are summarised in Table S1. Overall, three alkyl chain lengths ($i = 8$, 12, and 16) and two sets of EO units ($j = 6$ and 12) were combined. Table 2 displays the hydrophilic-lipophilic balance (HLB) [83] of these compounds calculated with Eq. 3.1:

$$HLB = 20 * \frac{M_h}{M} \tag{3.1}$$

where M_h is the molar mass of the hydrophilic segment and M is the molar mass of the surfactant covered in this study (values between 10 and 20 characterize water-soluble surfactants). Furthermore, the $C_{16}TAB$ surfactant was chosen to compare with the nonionic $C_{16}E_{12}$ and evaluate the impact of the charge in the detachment of hydrocarbons from silica-based surfaces.

Four 8%wt., 13%wt., 30%wt. and 60%wt. C_iE_j concentrations in aqueous solution were brought into contact with a silica surface covered by a layer of dodecane. All systems were built with Packmol and equilibrated prior the production runs along 2000 ns of simulation time at a temperature of 298 K. The final simulation snapshots are shown in Fig. 2, illustrating the diverse phases obtained and the extent of

Table 1
Micelle aggregation numbers for aqueous solutions of C_8E_6, $C_{12}E_6$, $C_{16}E_{12}$ and $C_{16}TAB$ surfactants obtained with MARTINI 2.2, MARTINI 3.0, and experimental data.

System	MARTINI 2.2	MARTINI 3.0	Experiments
C_8E_6	62[a]	53	32 [78], 51 [79]
$C_{12}E_6$	91[a]	111	110 [80], 144–180 [81]
$C_{16}E_{12}$	67[a]	83	152 [81]
$C_{16}TAB$	90 [21]	70	70–120 [82]

[a] Results obtained in Crespo et al. [30]

Table 2
Hydrophilic-lipophilic balance of the surfactants studied.

Surfactant	HLB
$C_{12}E_6$	13.0
C_8E_6	14.9
$C_{16}E_{12}$	14.5
C_8E_{12}	17.0
$C_{16}TAB$	21.4 [84]

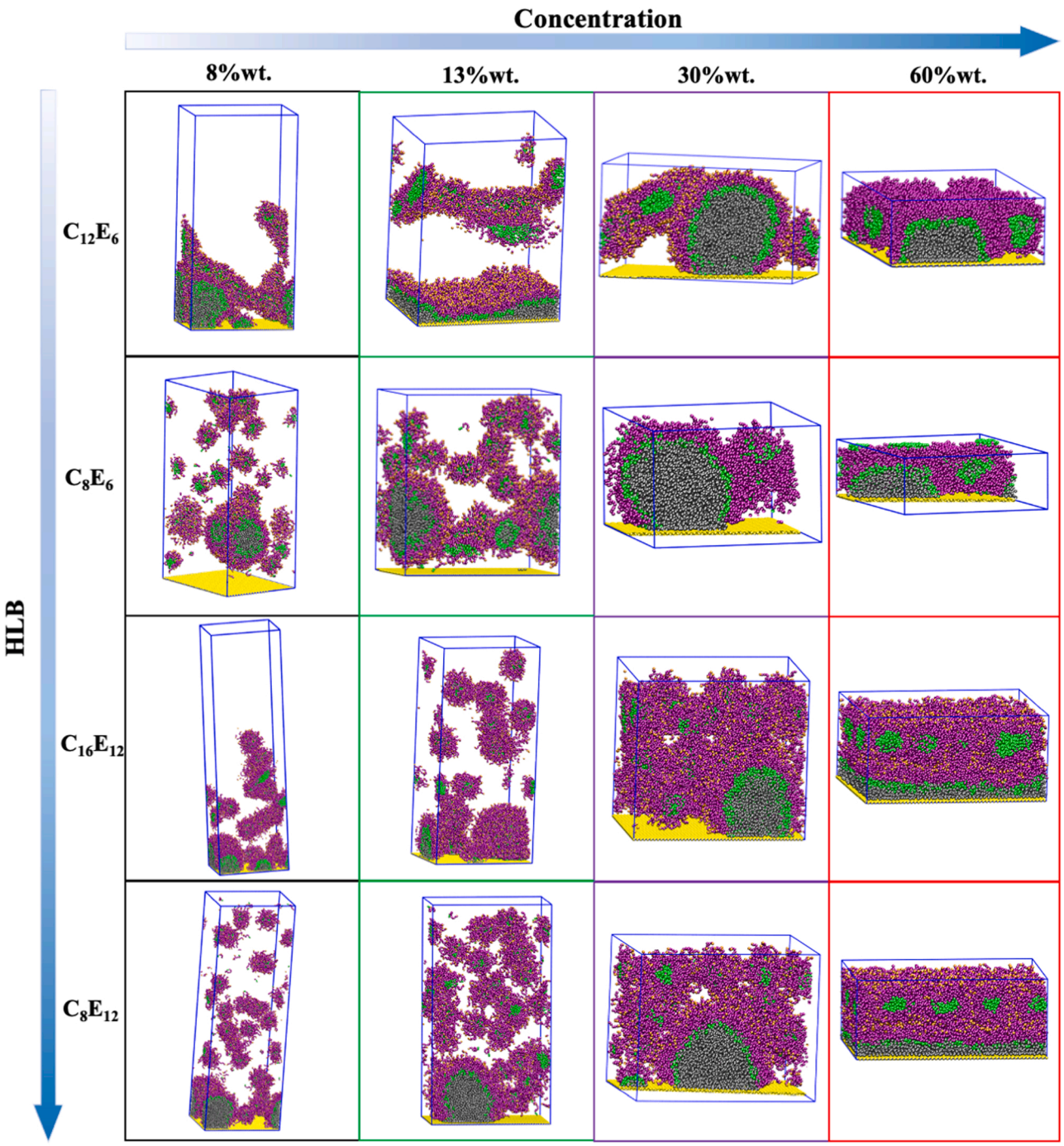

Fig. 2. CG-MD simulation snapshots obtained after 2000 ns of simulation time for 8%wt., 13%wt., 30%wt. and 60%wt. C_iE_j concentrations in aqueous solution with dodecane arranged over the silica surface. Green and purple colours represent the alkyl tail beads and EO units of C_iE_j, respectively. Dodecane is coloured grey and the silica surface in yellow. Some simulation boxes were split for the ease of visualisation and the size of some simulation boxes was scaled for a clearer comparison. Water molecules were removed for clarity.

dodecane detachment from the silica surface as a function of concentration and HLB.

The $C_{12}E_6$, with the lowest HLB, yielded rod-like micelles, partially removing dodecane from the surface in the 8%wt. solution, but the oil remained completely attached to the surface when the concentration was increased to 13%wt. However, further concentration increases to 30%wt. and 60%wt. resulted in a dodecane partial detachment, being wrapped inside prolate-shaped clusters, as can be seen in Fig. 2. When the HLB is increased with the C_8E_6 surfactant, a complete detachment was observed but only at relatively low concentrations, 8%wt. and 13% wt., as the dodecane was absorbed by spherical clusters homogeneously distributed in the water phase. At 30%wt. and 60%wt., the formation of relatively big clusters somehow hindered the extraction of dodecane that remained partially attached to the silica surface. Despite C_8E_6 and $C_{12}E_6$ entail similar HLB, the later yielded elongated structures at 8%wt. and 13%wt. in contrast with the spherical aggregates formed by C_8E_6. Similar behaviour was found when the alkyl chain and number of EO groups are duplicated, with the $C_{16}E_{12}$ surfactant, forming mainly spherical micelles at 8%wt. and 13%wt. and relatively big clusters at 30%wt. partially absorbing the dodecane. The hexagonal phase

obtained at 60%wt. somehow hindered the detachment of dodecane and remained completely attached and covered by a thin layer of $C_{16}E_{12}$ surfactant. Finally, by increasing the hydrophilic character of C_8E_6 with the addition of six EO groups, in C_8E_{12} (HLB ~ 17), the 8%wt. solution yielded spherical micelles with no trace of dodecane in the bulk phase but clusters partial wrapped dodecane, while attached to the silica surface. The clusters increased their size when the concentration was raised to 30%wt. but still linked to the silica surface with the partially absorbed dodecane as illustrated in Fig. 2. The 60%wt. solution yielded the same structure as in the $C_{16}E_{12}$ at this concentration, with the formation of a hexagonal phase in the water phase above the layered surfactant and dodecane structure attached to the surface. It seems that surfactants with relatively high HLB, such as the C_8E_{12}, yields the lowest efficiency at removing oil when compared with lower HLB solutions. Thus, there is an optimal HLB index (HLB ~ 15) for which oil recovery is optimal and any HLB increase or decrease results in reduced detachment.

The impact of the oil chain length was also analysed considering an eicosane layer above the silica surface. Fig. S1 shows the simulation snapshots after 2000 ns of simulation time for all the systems and concentrations displayed in Fig. 2. The hydrophobic $C_{12}E_6$ surfactant formed rod-like micelles in the water phase overall concentrations but the eicosane remained completely attached to the surface except for the 60% wt. solution where it was partially wrapped inside the gyroid like phase (Fig. S1). Contrary to was observed for dodecane (except for the 13%wt. solution), the eicosane remained as a layer covering the entire silica surface with a thin layer of surfactant in 8%wt., 13%wt. and 30% wt. solutions. In the presence of eicosane, the C_8E_6 surfactant could not completely dissociate it from the surface in the diluted 8%wt. and 13% wt solutions. Instead, spherical clusters, partially wrapping eicosane from the surface but still attached, were found in equilibrium with small micelles in the water phase. Some of them absorbed eicosane as can be noticed in Figs. S1 and S2 (highlighted with red circles for 8%wt. and 13%wt. systems). The 60%wt. solution was not able to detach eicosane from the surface but formed a undulated C_8E_6 layer involving the eicosane, suggesting that a partial detachment could occur if the simulation time is extended. Notably, the $C_{16}E_{12}$ resembled the results found with the more hydrophobic $C_{12}E_6$ surfactant, exhibiting rod-like micelles with no trace of eicosane detachment overall concentrations as can be seen in Fig. S1. Only the 60%wt. solution yielded a hexagonal phase as the solution with dodecane (Fig. 2). Finally, the C_8E_{12} surfactant generated spherical clusters, partially separating the eicosane from the surface in the 8%wt., 13%wt. and 30%wt. solutions whereas the 60%wt. solution resembled the hexagonal structure formed in the solution with dodecane. From the above results, it seems that when the length of the hydrocarbon chain is increased, the detachment process becomes more difficult, perhaps affected by the difficulty of breaking stronger hydrophobic-hydrophobic interactions between packed eicosane molecules. This assumption relies on the fact that the observed surfactant phase behaviour of the analysed C_iE_j surfactants was analogous to the solutions with dodecane but with eicosane, the detachment process seems to take longer.

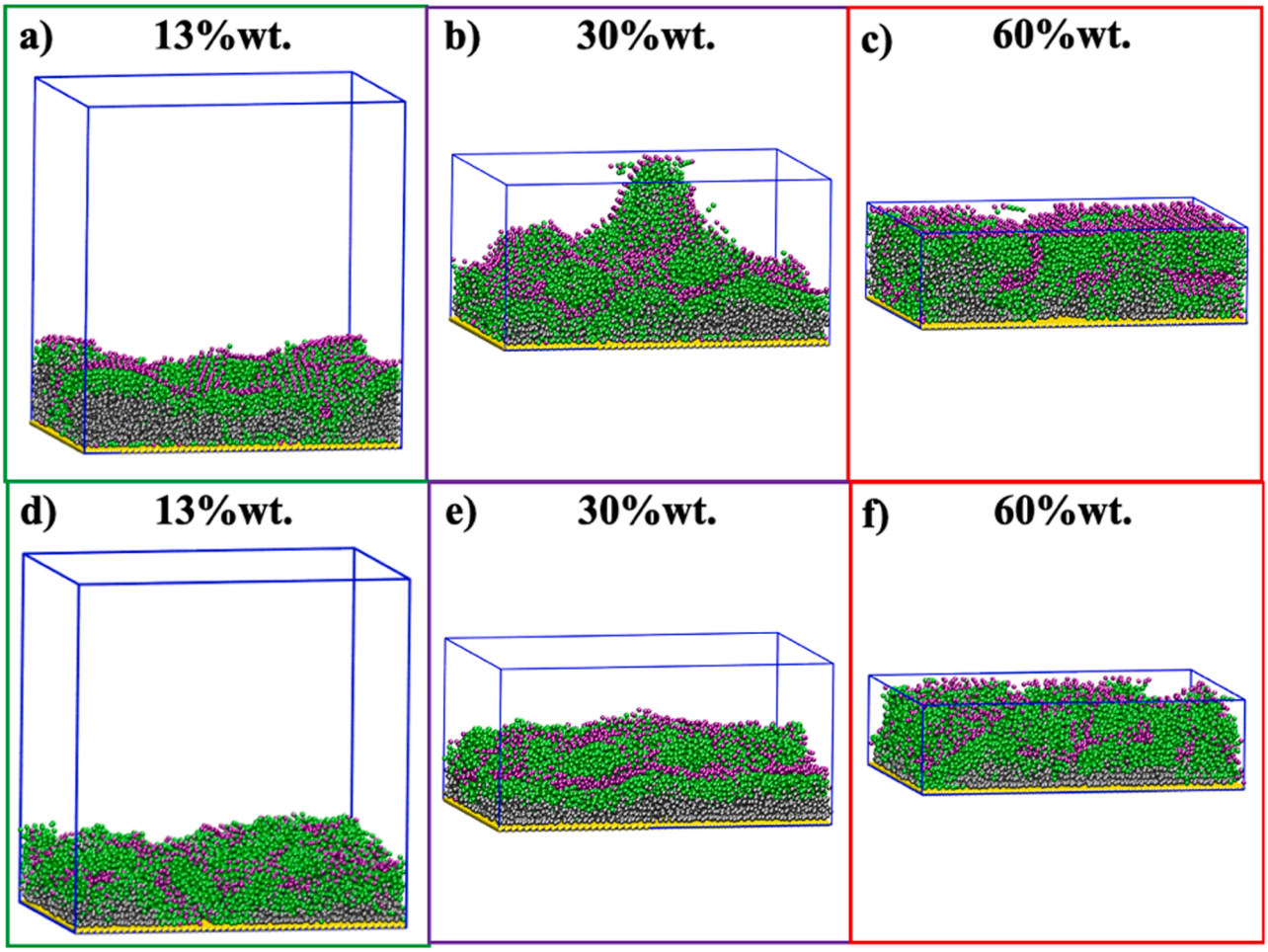

Fig. 3. CG-MD simulation snapshots obtained after 2000 ns of simulation time for 13%wt., 30%wt. and 60%wt. C_{16}TAB aqueous solutions with dodecane (a-c) and eicosane (d-f). The colour code is the same as in Fig. 2 where the alkyl tails and the ammonium charged centre of C_{16}TAB are coloured in green and purple, respectively. Water molecules and bromide counterions were removed for clarity.

The impact of the surfactant charge was investigated with the $C_{16}TAB$, which contains the same alkyl tail length as in the $C_{16}E_{12}$ surfactant, but the hydrophilic moiety is an ammonium charged centre. Three concentrations, 13%wt., 30%wt., and 60%wt., were studied and the final structures after 2000 ns are displayed in Fig. 3. This figure reveals that cationic surfactants might not be the most suitable candidates for EOR processes as both, the $C_{16}TAB$ and the oil (both, dodecane or eicosane) remained well attached to the silica surface. Overall concentrations, the $C_{16}TAB$ formed gyroid-like structures, partially wrapping the dodecane (Fig. 3 a-c) or eicosane (Fig. 3 d-f) and arranged densely packed over the silica surface, especially in the systems with eicosane. Conversely to what was found in nonionic surfactants, no traces of $C_{16}TAB$ aggregates were found in the water phase.

Figs. S3 and S4 display the surfactant and oil interactions when the silica surface is not present. Fig. S3 shows that spherical aggregates wrapping dodecane were predominant, from small micelles at 8%wt. and 13%wt. concentrations to relatively large prolate shaped aggregates in 30%wt. and 60%wt. solutions. Surfactants with larger alkyl tails such as $C_{12}E_6$ or $C_{16}E_{12}$ retained more oil due to their higher hydrophobic volume, exhibiting slightly bigger aggregates, more noticeable at higher concentrations (30%wt. and 60%wt.) when compared with the hydrophilic surfactants such as C_8E_6 or C_8E_{12}. The cationic $C_{16}TAB$ formed fewer and larger aggregates when compared with the nonionic surfactants and, at higher concentrations, a hexagonal phase was formed with dodecane moieties located inside the rods. Fig. S4 displays the same surfactant solutions with eicosane, denoting that spherical micelles still prevail at low concentrations, but yielding clusters as soon as the surfactant concentration is increased. All eicosane molecules were incorporated by the surfactant assemblies, increasing the aggregate size distribution due to the increased hydrophobic volume when compared with the dodecane. The $C_{16}TAB$ exhibited spherical micelles with absorbed eicosane in the 13%wt. solution whilst clusters at 30%wt. and 60%wt., in contrast with the solutions with dodecane, where micellar rods were present at higher concentrations. It is interesting to note that, unlike the nonionic counterparts, the behaviour of the cationic $C_{16}TAB$ is substantially different in the presence of a silica surface, where the surfactant and oil remained densely packed, and no bulk aggregates were observed. It seems that the more hydrophilic nature of the ammonium charged group of $C_{16}TAB$, when compared with the EO groups of C_iE_j surfactants, results in stronger interactions with the polar silica surface.

3.2. Solvent accessible surface area analysis

The trend displayed by the solvent accessible surface areas, SASA, along the simulation can provide significant information about when and how the phase transition occurs, including the detachment of the oil from the silica surface. An early increase of SASA for surfactant EO groups means that the initial surfactant layer placed over the dodecane undergoes a morphologic transformation which, in our case, corresponds to the formation early small micelles. When the early micelles are formed, the EO groups occupy the outer shells and the contact area with the water subphase is increased. When an increase of SASA for surfactant EO groups coincides with a decrease of the SASA of oil (dodecane or eicosane), the originally arranged layer of oil over the silica surface abandons this configuration to be absorbed and encapsulated by the surfactant aggregate, thus losing access to water as it was wrapped by the hydrophobic core of the aggregate.

The SASA profiles of the dodecane (solid lines) and the EO groups of $C_{12}E_6$ (dashed lines), displayed in Fig. 4, denote that the partial detachment of dodecane in the 8%wt. solution arose at ~ 400 ns. Fig. S5a shows the phases before and after the partial detachment process at 350 and 650 ns. Fig. 4 also displays the gain of access to water of EO groups (SASA dashed lines in black) corresponding to the concurrent loss of hydration of the dodecane (black solid lines). The 13%wt. solution was unable to remove the dodecane and both SASA profiles (EO and dodecane) remained mostly constant along the simulation. Only a quick SASA increase at the beginning denoted the formation of the rod-like structures inside the water phase depicted in Fig. 2. The 30% wt. system partially detached the dodecane from the surface after 1200 ns, denoting the formation of clusters attached to the surface and partially wrapping the dodecane (snapshot insets of Fig. S5a). A dodecane partial detachment occurred early in the 60%wt. system as suggested by the increase of the SASA of dodecane and EO groups shown in Fig. 4. Fig. S5a shows a ripped structure at 50 ns, followed by the formation of a gyroid-like structure after 350 ns. This phase was formed while the dodecane was being extracted, as denoted by the constant value of SASA for EO groups (red dashed line) as shown in Fig. 4. Fig. S5b displays the SASA of eicosane for the systems displayed in Fig. S1, where only the 60%wt. solution showed some eicosane detachment (inset at 50 ns) denoting an important loss of access to water as the oil was partially wrapped by the gyroid structure (inset at 700 ns).

The SASA profiles for C_8E_6 (Fig. 4) present two different regimes, below and above 400 ns, for almost all systems, suggesting that the initial dodecane detachment occurred at similar stages and denoting a weak impact of the surfactant concentration. In 8%wt. and 13%wt. solutions (black and green, respectively), the constant dodecane SASA (solid lines) during the first 300 ns (150 ns insets in Fig. S6a), corresponds to a stable thin layer of C_8E_6 over the attached dodecane. The formation of early C_8E_6 micelles also occurred as the quick increase of SASA of EO groups in C_8E_6 (dashed lines) suggests. At 300 ns, the SASA of dodecane quickly dropped (with simultaneous SASA increase for EO groups) for both concentrations, denoting the initial stage of partial detachment of dodecane from the silica surface and the formation of micelles as shown in Fig. S6a (450 ns). The second slope of the SASA of C_8E_6 EO groups between 400 and 600 ns at both concentrations (dashed lines) corresponds to the total dodecane absorption by C_8E_6 micelles whose sizes remained constant. The SASA of dodecane for the 30%wt. solution (solid purple) rapidly dropped (above 2 ns) pointing towards a quick partial detachment from the silica surface and absorption by relatively large C_8E_6 cluster formation as denoted by the smooth increase of the SASA of EO C_8E_6 groups (dashed purple) – details in insets with purple arrows at 2 and 300 ns in Fig. S6a. When the C_8E_6 concentration is increased to 60%wt. (red lines), Fig. 4 shows that the SASA of dodecane and EO C_8E_6 groups increased, displaying analogous values, in contrast with what was observed in the first 150 ns at lower concentrations. Both the dodecane and C_8E_6 EO groups gained access to the water, indicating that some dodecane was barely disrupted from the surface by the C_8E_6 perforated layered structure formed at 800 ns (Fig. S6a). This phase remained constant until 1300 ns where the SASA of dodecane exhibited a subtle maximum, indicating an increase in access to water since more dodecane was wrapped from the surface. The lack of micelle formation can be noticed by the difference between the C_8E_6 SASA for EO groups (dashed red) ~ 1.65 nm^2 in the 60%wt. solution and those values for the diluted ones ~ 2.0 nm^2 as can be seen in Fig. 3. Fig. S6b shows the SASA of eicosane for the systems evaluated in Fig. S1, where the decrease of SASA in the 8%wt. and 13%wt. solutions, corresponds to a quick partial detachment of eicosane from the silica surface. A layer-to-cluster transition, partially wrapping eicosane, was observed as shown in the insets of Fig. S6b (highlighted by the black and green arrows for 8%wt. and 13%wt. solutions, respectively).

The SASA of $C_{16}E_{12}$ solutions also revealed two regimes, but less evident than for C_8E_6 as can be noticed in Fig. 4. The SASA of dodecane showed a quick increase (first 100 ns) for 8%wt., 13%wt. and 30%wt. concentrations (solid lines Fig. 4) where the water penetrated the initial $C_{16}E_{12}$ layer, reaching the dodecane film. Then, the SASA of dodecane dropped (between 200 and 400 ns), indicating a loss of contact between dodecane and water due to the absorption by $C_{16}E_{12}$ clusters as denoted in the simulation insets of Fig. S7a (black, green, and purple arrows). The 60% wt. solution quickly formed spherical and rod-like micellar structures in the water phase (20 ns inset in Fig. S7a) above the $C_{16}E_{12}$ and dodecane layers attached to the silica surface. Consistently, the

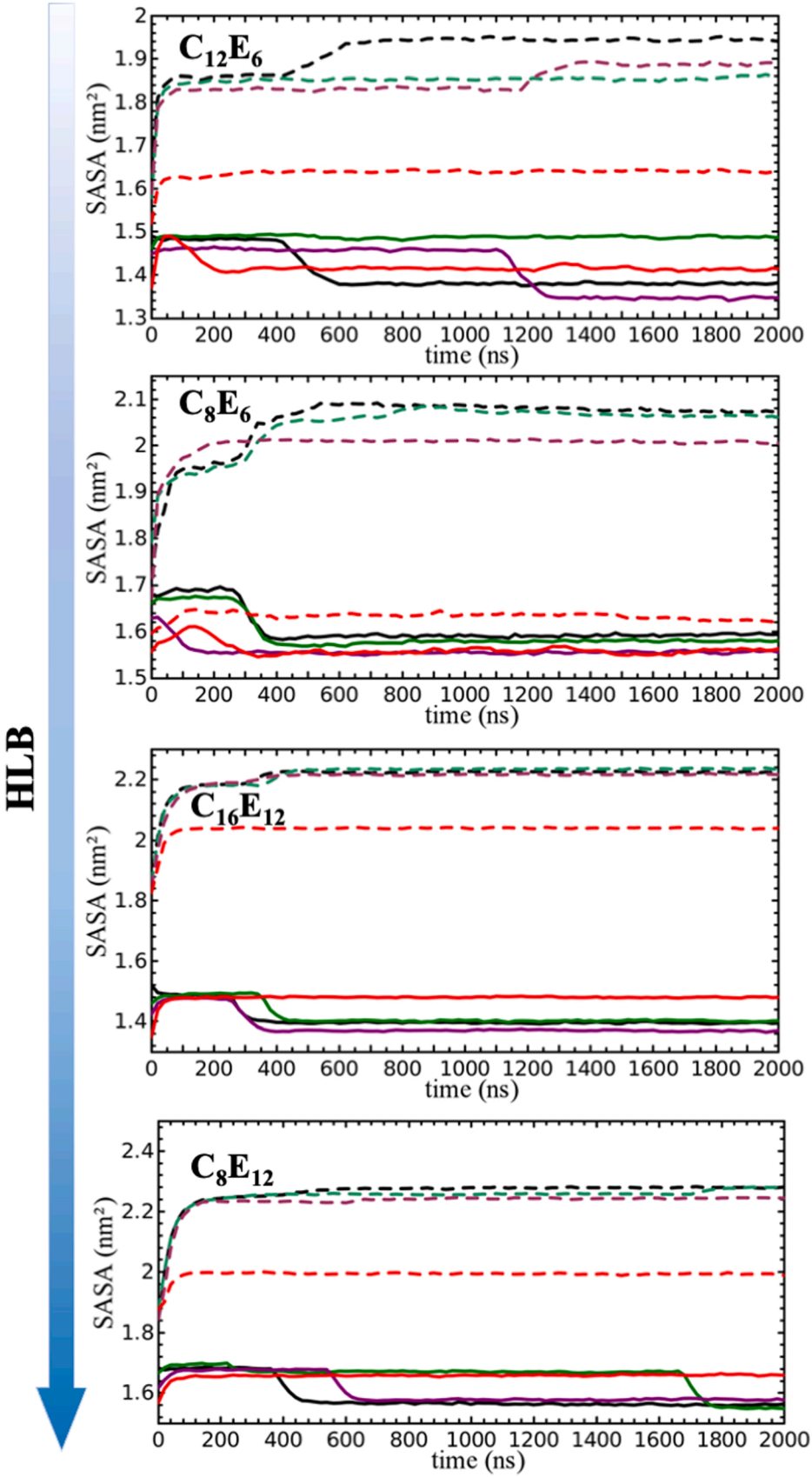

Fig. 4. Solvent accessible surface area (SASA) profiles of EO groups in C_iE_j (dashed) and dodecane (solid) overall C_iE_j concentrations after 2000 ns simulation time. The colour code for 8%wt., 13%wt., 30%wt. and 60%wt. C_iE_j concentrations is black, green, purple, and red, respectively.

SASA of $C_{16}E_{12}$ EO groups (dashed lines in Fig. 4) resembles the trend observed for C_8E_6 except for the lack of a second slope since the $C_{16}E_{12}$ was unable to detach the dodecane completely and the clusters remained linked to the silica surface for the 8%wt., 13%wt. and 30%wt. solutions. The increase of SASA of dodecane for the 60%wt. results from the formation of rod-like structures, remaining unchanged until the end of the simulation, also denoted by the continuous SASA of $C_{16}E_{12}$ EO groups (red dashed line). In contrast with the C_8E_6, the SASA of $C_{16}E_{12}$ EO groups denoted the formation of a hexagonal phase (Fig. 2) with increased access to water. Fig. S7b shows the SASA of the systems with eicosane displaying a completely different picture. The SASA of eicosane at 8%wt., 13%wt. and 30%wt. resembled the initial stages of aggregation observed in the systems with dodecane (bulky aggregates above the surfactant and oil layers) but remained in equilibrium in contrast with the layer-to-cluster transition observed in the system with dodecane (simulation snapshots of Fig. S7a). Conversely, the 60%wt. solution with eicosane resembled the formation of a hexagonal structure observed in the system with dodecane, with a very similar SASA profiles (Fig. S7).

The SASA of C_8E_{12} surfactant are shown in Fig. 4 indicating that the most hydrophilic nonionic surfactant was less efficient on detaching the dodecane, despite yielding similar structures as can be perceived in Fig. 2. The SASA of dodecane in Fig. 4 shows that the 8%wt., 13%wt. and 30%wt. C_8E_{12} solutions took longer, 400, 1700, and 600 ns, respectively, to partially separate the dodecane from the silica surface. The formation of the spherical clusters proceeded slower when compared with the more hydrophobic nonionic surfactants, as suggested by the smooth increase of the SASA of C_8E_{12} EO groups (dashed lines in Fig. 4). Fig. S8a shows the configurations before and after the partial desorption of dodecane, denoting layer-to-cluster transitions also observed in the other nonionic surfactants. The SASA of dodecane and EO groups in the 60% wt. solution resembled the profiles obtained for $C_{16}E_{12}$, but lower access to water when compared with the $C_{16}E_{12}$ solution. This discrepancy is a consequence of subtle differences in the hexagonal phase that only a careful analysis of the simulation snapshots displayed in Fig. 2 can discern. In fact, the 60%wt. $C_{16}E_{12}$ solution yielded a hexagonal phase (Fig. S9a) but a cubic micellar solution in C_8E_{12} (Fig. S9b). The $C_{16}E_{12}$ rods entails a higher surface in contact with water when compared with the rods and micelles observed in C_8E_{12}.

The SASA of eicosane shown in Fig. S8b resembles the profiles obtained for dodecane, but characterized by more obvious shifts towards lower SASA values when the eicosane was partially detached. This suggests that bigger structures with more exposed surface to the water were formed in presence of eicosane, likely due to the increase of the hydrophobic volume of the absorbed eicosane. In fact, the averaged shift of SASA of eicosane in the 8%wt., 13%wt. and 30%wt. solutions ~ 0.25 nm^2 almost double the water contact area compared with the solution of dodecane ~ 0.11 nm^2 (Fig. S8). Remarkably, the partial detachment of eicosane occurred sooner in the 8%wt. and 30%wt. solutions (200 ns and 800 ns, respectively) than in the 13%wt. (1700 ns) system as can be seen in Fig. S8b. The 60%wt. solution also replicated the scenario found with dodecane, with no eicosane detachment whilst the formation of a C_8E_{12} hexagonal phase as shown in Fig. S1 and

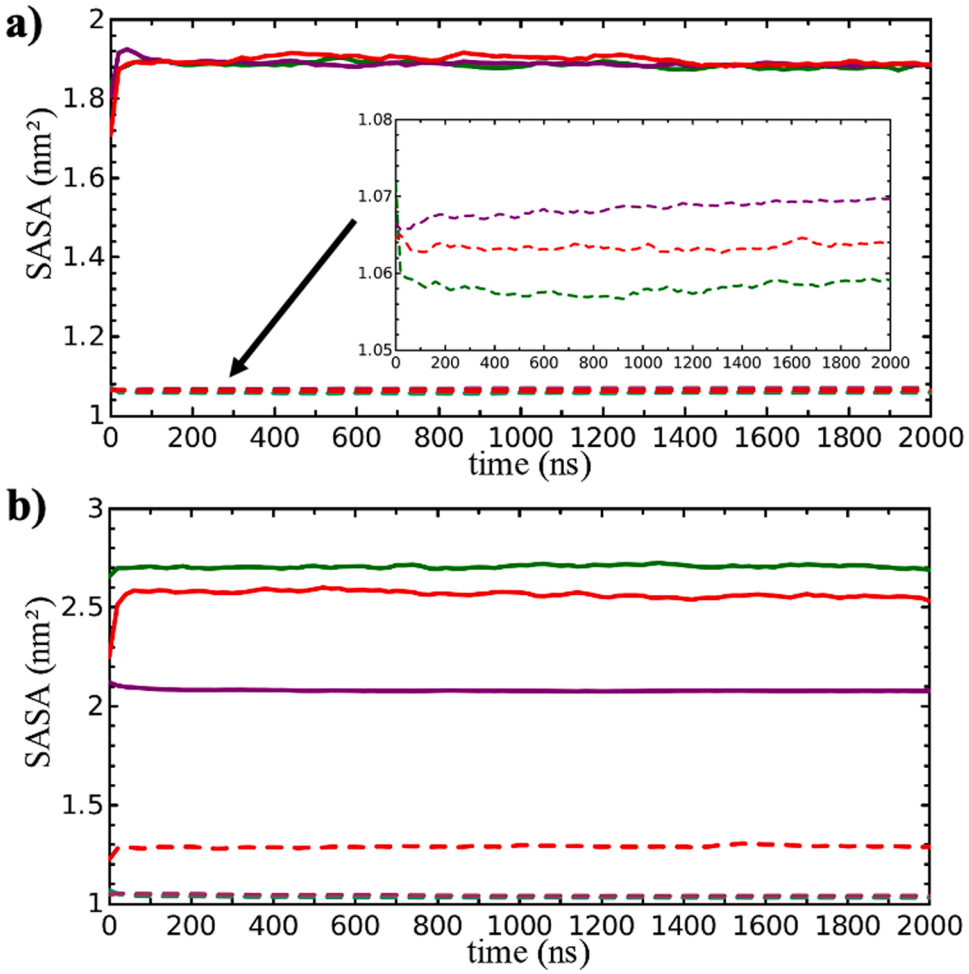

Fig. 5. Solvent accessible surface area (SASA) profiles of dodecane (a) and eicosane (b) besides their C_{16}TAB ammonium centres for 13%wt., 30%wt., and 60%wt. concentrations after 2000 ns simulation time. The colour code for 13%wt., 30%wt. and 60%wt. C_{16}TAB concentrations are green, purple, and red, respectively. The inset in Fig. 5**a** shows an enhanced perspective.

denoted in the simulation snapshot inset of Fig. S8b (1100 ns).

Fig. 5**a** displays the SASA of the C_{16}TAB charged ammonium headgroups (solid lines) and the dodecane (dashed lines) for each concentration. All of them exhibited identical patterns with an initial increase of the SASA of dodecane overall concentrations, denoting that the water rapidly penetrated the C_{16}TAB layer giving access to water to reach the dodecane. The constant value of the SASA of C_{16}TAB ammonium charge centres indicates that the gyroid phase remained stable along the simulation as displayed in Fig. 3. Fig. 5b shows the SASA profiles for the solutions with eicosane, which seemed more sensitive to the changes in C_{16}TAB concentration. The differences observed are associated with internal structure of the gyroid phases, likely due to the formation of larger channels throughout the C_{16}TAB mesophase. In fact, more compacted structures were found in the solutions with dodecane.

3.3. Overall outcomes

The results obtained in the simulations suggest that, along 2000 ns of simulation time, the C_8E_6 surfactant yielded the best performance on the extraction of dodecane from silica-based surfaces, although less efficient when detaching eicosane. The increased alkyl chain implies a higher energy penalty for breaking hydrophobic-hydrophobic interactions between eicosane molecules. Conversely, the alkyl chain of dodecane and the alkyl tail length of C_8E_6 are similar and, from an energetic point of view, breaking hydrophobic-hydrophobic interactions of dodecane-dodecane pairs by C_8E_6 (alkyl tail-dodecane) is more energetically favourable. Increasing the hydrophilic content with the C_8E_{12} surfactant did not improve the oil recovery, displaying partial detachments and some degree of association to the silica surface. Maintaining the hydrophilic content of C_8E_6 and increasing the hydrophobic character with the $C_{12}E_6$ surfactant, also resulted in partial detachment of oil, similarly to the C_8E_{12} system. Increasing both, the hydrophilic and hydrophobic content of C_8E_6 with the $C_{16}E_{12}$ surfactant, yielded similar oil removal rates to $C_{12}E_6$ and C_8E_{12}. Even though the $C_{16}E_{12}$ possesses the same HLB as the C_8E_6, the increased molecular weight in $C_{16}E_{12}$ seems to play an important role in the oil detachment, likely due to its lower diffusion besides the phase behaviour. Fig. 2 illustrates the impact of the HLB, molecular weight and concentration of the surfactant in the detachment of dodecane (eicosane in Fig. S1) pointing that these three variables are crucial when surfactants are used for EOR. Finally, the impact of charge in oil removal was evaluated with the C_{16}TAB cationic surfactant. Three concentrations were evaluated with dodecane or eicosane layers above the silica surface. Overall, the C_{16}TAB could only partially detach some dodecane or eicosane from the silica surface, forming packed gyroid-like structures with absorbed oil inside the branches but completely linked to the surface.

The surfactant aqueous solutions and oil without the silica surface (Figs. S3 and S4 for the dodecane and eicosane solutions, respectively) exhibited mainly spherical aggregates with different sizes depending on the surfactant nature and concentration. Surfactants with longer alkyl tails, such as $C_{12}E_6$ or $C_{16}E_{12}$, yielded bigger aggregates, retaining more oil due to the increased hydrophobic volume. The dodecane or eicosane absorption was more obvious at higher concentrations (30%wt. and 60%wt.). The more hydrophilic surfactants such as C_8E_6 or C_8E_{12} assembled into smaller aggregates, all of them with absorbed oil. The cationic C_{16}TAB produced larger aggregates, even when compared with similar alkyl chain lengths such as in $C_{12}E_6$ or $C_{16}E_{12}$ nonionic surfactants, yielding a hexagonal-like phase with oil moieties located inside the rods at higher concentrations. For all systems and concentrations, the aggregates with absorbed eicosane exhibited greater sizes when compared with the systems with absorbed dodecane due to the difficulty to accommodate a larger linear moiety. Due to the imposed limit in the simulation time, only the initial stages were compared, and longer simulation times could tell us more on whether the bulkier aggregates converge into larger ones or form other structures. However, due to the number of analysed systems at different concentrations, the limited computational resources available imposed a restriction in the simulation time. Even though, the purpose of this study aimed to understand the performance of typical surfactants used in EOR and the results obtained provided some insight on how the surfactant phase behavior impact the detachment of oil. An additional analysis was performed via the number density profiles of selected moieties for the nonionic C_iE_j and cationic C_{16}TAB solutions analysed in this study along the axis in the normal direction to the silica surface (Figs. S10-S14). A detailed discussion can be found in the supplementary material section shedding light into the internal structure of the simulation boxes for the last 500 ns of simulation time. The density profiles can be helpful to understand the phases revealed in Fig. 2 and S1 besides the interpretation of the SASA profiles shown in Figs. 4, 5 S1, S5-S8.

4. Conclusions

A novel coarse-grained molecular dynamics computer simulation framework, based on MARTINI 3.0, was developed to analyse the impact of the phase behaviour of aqueous solutions of nonionic C_iE_j and cationic C_{16}TAB surfactants in the removal of oil compounds from silica-based surfaces. The silica surface model was validated against atomistic simulations and experimental data found in the literature whereas micellar distributions were used for the aqueous solutions of C_iE_j and C_{16}TAB surfactants. Remarkably, the MARTINI 3.0 yielded better predictions for the micellar size distribution of C_iE_j and C_{16}TAB aqueous solutions compared with results obtained with MARTINI 2.2. Four C_iE_j (C_8E_6, C_8E_{12}, $C_{12}E_6$, $C_{16}E_{12}$) and the C_{16}TAB surfactant were simulated at different concentrations to evaluate the removal of either, dodecane or eicosane from a silica surface. Simulations revealed that, after 2000 ns of simulation time, only the C_8E_6 surfactant completely retrieved the dodecane from the silica surface but at relatively low concentrations (8%wt. and 13%wt.) where spherical clusters were formed. At higher concentrations, elongated phases emerged and the dodecane was only partially detached from the surface. The eicosane was only partially detached overall C_8E_6 surfactant concentrations. The increased alkyl chain length raises the energy barrier for breaking hydrophobic-hydrophobic interactions between eicosane moieties, hindering their absorption by C_8E_6 aggregates. Conversely, the alky chain length of C_8E_6 and dodecane are similar and the dodecane seems more prone to be retrieved.

Varying the HLB of C_iE_j surfactants (extending the hydrophilic, hydrophobic or both segments in C_8E_{12}, $C_{12}E_6$ and $C_{16}E_{12}$, respectively) only yielded partial or no detachment of dodecane or eicosane. Thus, the C_8E_6 entails an ideal HLB ($\sim$ 15) and, as argued below, a relatively low molecular weight (noticeable inferior to $C_{16}E_{12}$) for a quick water channel formation and penetration into dodecane or eicosane layers to retrieve them from the silica surface. This agrees with previous atomistic simulation results where a greater surfactant mobility seems to promote the formation of water channels through the oil layer.[15] In fact, $C_{16}E_{12}$ with the same HLB but high higher molecular weight, could not improve the oil detachment when compared to C_8E_6. $C_{16}E_{12}$ solutions formed elongated micellar structures that hindered the oil detachment as it was also observed in C_8E_{12}. Certainly, similar HLB can yield different mesophases, noticeably affecting the performance of oil removal. By decreasing the HLB below 15 (increasing hydrophobic content), $C_{12}E_6$ solutions delayed the formation of water channels and further infiltration to the silica surface likely due to the quick formation of flattened structures as well. Raising the HLB above 15 (increase of the hydrophilic content), C_8E_{12} solutions rapidly formed micelles but their hydrophilic character yielded weaker interactions with the oil layer, delaying the formation of water channels.

Accessible solvent surface areas (SASA) for oil moieties and the hydrophilic groups of the surfactants were used to determine the promptness of the water channel formation into the dodecane or eicosane layers overall concentrations and surfactants. The C_8E_6 displayed more abrupted changes in the SASA profiles, denoting a quick surfactant

and water penetration into the dodecane layer and a complete dodecane absorption by C_8E_6 micelles at low concentrations, losing effectiveness when the surfactant concentration is raised where flatter structures were formed. Eicosane layer disruptions from the silica surface proceeded slower, as can be noticed by the smoother variations of SASA profiles, overall nonionic surfactants, and concentrations, where only partial detachments were achieved. The SASA profiles for C_8E_{12}, $C_{12}E_6$, $C_{16}E_{12}$ surfactants showed that the changes in the SASA profile occurred later, denoting a delay in water channel formation when compared with the C_8E_6.

Our simulations also revealed that cationic surfactants could not be appropriate for dodecane or eicosane recovery as both oil and C_{16}TAB remained completely attached to the silica surface overall concentrations. This is in contrast with Tang et al.[15] results where they argued that cationic surfactants promptly formed water channels in the dodecane layer when compared with nonionic surfactants. Nevertheless, the nonionic and cationic surfactants, OP-10 and DTAB, respectively, were different from those used in our study.

Interestingly, in absence of a silica surface, the C_{16}TAB was the most efficient at retrieving dodecane or eicosane from the aqueous solutions when compared with the nonionic C_iE_j surfactants. This certainty suggests that the C_{16}TAB can quickly form water channels in the oil layer as found by Tang et al. and noticed in our C_{16}TAB SASA profiles for dodecane (early and abrupt changes in the profile). However, the quick C_{16}TAB self-assembly coupled with the strong interactions between the ammonium C_{16}TAB charged headgroups with the polar silica surface could generate a strong attraction between them, and therefore retaining the oil at the silica surface. A further investigation with other cationic surfactants could provide more clues into this issue.

The results obtained in this study are very promising and demonstrate the capabilities of MARTINI 3.0 and CG-MD simulations to tackle multi-component systems used in industry and the importance of phase formation in EOR processes. Future work will focus on anionic surfactants and more complex oils besides the impact of salt that is commonly found in seabed reservoirs. Furthermore, CG-MD simulations will aid in evaluating the high pressures and temperatures used in chemical EOR processes that are difficult to reproduce in the laboratory.

CRediT authorship contribution statement

Germán Pérez Sánchez: Investigation, Data Curation, Writing – original draft; **Filipa Costa**: Investigation, Writing – original draft; **Gonçalo M. C. Silva** – review & editing; **Manuel M. Piñeiro** – review & editing; **João A. P. Coutinho** – Conceptualization, Supervision, Writing – review & editing.

Declaration of Competing Interest

The authors declare that they have no known competing financial interests or personal relationships that could have appeared to influence the work reported in this paper.

Data Availability

Data will be made available on request.

Acknowledgments

This work was developed within the scope of the project CICECO-Aveiro Institute of Materials, UIDB/50011/2020, UIDP/50011/2020 & LA/P/0006/2020, financed by national funds through the FCT/MEC (PIDDAC). G. Pérez-Sánchez acknowledges the national funds (OE), through FCT – Fundação para a Ciência e a Tecnologia, I.P., in the scope of the framework contract foreseen in the numbers 4, 5 and 6 of the article 23, of the Decree-Law 57/2016, of August 29th, changed by Law 57/2017, of July 19th. Simulations were performed at the OBLIVION Supercomputer managed by the HPC Centre of the University of Évora and acquired under the "Enabling Green E-science for the SKA Research Infrastructure (ENGAGE SKA)", reference POCI-01-0145-FEDER-022217, funded by COMPETE 2020 and Foundation for Science and Technology (FCT), Portugal. The simulations were funded by the FCT program "Concurso de Projetos de Computação Avançada - 2ª Edição" with the project reference CPCA/A1/394985/2021.

Appendix A. Supporting information

Supplementary data associated with this article can be found in the online version at doi:10.1016/j.colsurfa.2023.131583.

References

[1] Short-term energy outlook, U.S. Energy Inf. Adm. , 2021. https://www.eia.gov/outlooks/steo/, (n.d.). https://www.eia.gov/outlooks/ieo/production/sub-topic-01.php (accessed November 7, 2022).
[2] W.B. Gogarty, Status of surfactant or micellar methods, J. Pet. Technol. 28 (1976) 93–102, https://doi.org/10.2118/5559-PA.
[3] R.N. Healy, R.L. Reed, Immiscible microemulsion flooding, Soc. Pet. Eng. J. 17 (1977) 129–139, https://doi.org/10.2118/5817-PA.
[4] D.F. Boneau, R.L. Clampitt, A surfactant system for the oil-wet sandstone of the North Burbank Unit, J. Pet. Technol. 29 (1977) 501–506, https://doi.org/10.2118/5820-PA.
[5] V. Alvarado, E. Manrique, Enhanced oil recovery: an update review, Energy 3 (2010) 1529–1575, https://doi.org/10.3390/en3091529.
[6] E.J. Gudiña, L.R. Rodrigues, J.A. Teixeira, J.F. Pereira, J.A. Coutinho, SPE 154598 Biosurfactant producing microorganisms and its application to Enhance Oil Recovery at lab scale, 2012. ⟨http://www.ncbi.nlm.nih.gov⟩.
[7] O. Massarweh, A.S. Abushaikha, The use of surfactants in enhanced oil recovery: a review of recent advances, Energy Rep. 6 (2020) 3150–3178, https://doi.org/10.1016/j.egyr.2020.11.009.
[8] G. Lemahieu, J.F. Ontiveros, N. Terra Telles Souza, V. Molinier, J.-M. Aubry, Fast and accurate selection of surfactants for enhanced oil recovery by dynamic salinity-phase-inversion (SPI), Fuel 289 (2021), 119928, https://doi.org/10.1016/j.fuel.2020.119928.
[9] P. Becher, Microemulsions and related systems: formulation, solvency, and physical properties (surfactant science series, Vol. 30), J. Dispers. Sci. Technol. 11 (1990) 431–432, https://doi.org/10.1080/01932699008943264.
[10] Z. Liu, G. Zhao, M. Brewer, Q. Lv, E.J.R. Sudhölter, Comprehensive review on surfactant adsorption on mineral surfaces in chemical enhanced oil recovery, Adv. Colloid Interface Sci. 294 (2021), https://doi.org/10.1016/j.cis.2021.102467.
[11] J.J. Sheng, Optimum phase type and optimum salinity profile in surfactant flooding, J. Pet. Sci. Eng. 75 (2010) 143–153, https://doi.org/10.1016/j.petrol.2010.11.005.
[12] K. Mohan, R. Gupta, K.K. Mohanty, Wettability altering secondary oil recovery in carbonate rocks, Energy Fuels 25 (2011) 3966–3973, https://doi.org/10.1021/ef200449y.
[13] R. Rostami Ravari, S. Strand, T. Austad, Combined surfactant-enhanced gravity drainage (SEGD) of oil and the wettability alteration in carbonates: the effect of rock permeability and interfacial tension (IFT), Energy Fuels 25 (2011) 2083–2088, https://doi.org/10.1021/ef200085t.
[14] W. Wu, J. Pan, M. Guo, Mechanisms of oil displacement by ASP-foam and its influencing factors, Pet. Sci. 7 (2010) 100–105, https://doi.org/10.1007/s12182-010-0012-1.
[15] J. Tang, Z. Qu, J. Luo, L. He, P. Wang, P. Zhang, X. Tang, Y. Pei, B. Ding, B. Peng, Y. Huang, Molecular dynamics simulations of the oil-detachment from the hydroxylated silica surface: effects of surfactants, electrostatic interactions, and water flows on the water molecular channel formation, J. Phys. Chem. B 122 (2018) 1905–1918, https://doi.org/10.1021/acs.jpcb.7b09716.
[16] L.S. de Lara, M.F. Michelon, C.R. Miranda, Molecular dynamics studies of fluid/oil interfaces for improved oil recovery processes, J. Phys. Chem. B 116 (2012) 14667–14676, https://doi.org/10.1021/jp310172j.
[17] Q. Liu, S. Yuan, H. Yan, X. Zhao, Mechanism of oil detachment from a silica surface in aqueous surfactant solutions: molecular dynamics simulations, J. Phys. Chem. B 116 (2012) 2867–2875, https://doi.org/10.1021/jp2118482.
[18] S. Yuan, S. Wang, X. Wang, M. Guo, Y. Wang, D. Wang, Molecular dynamics simulation of oil detachment from calcite surface in aqueous surfactant solution, Comput. Theor. Chem. 1092 (2016) 82–89, https://doi.org/10.1016/j.comptc.2016.08.003.
[19] E. Lowry, M. Sedghi, L. Goual, Molecular simulations of NAPL removal from mineral surfaces using microemulsions and surfactants, Colloids Surf. A: Physicochem. Eng. Asp. 506 (2016) 485–494, https://doi.org/10.1016/j.colsurfa.2016.07.002.
[20] I.-C. Chen, M. Akbulut, Nanoscale dynamics of heavy oil recovery using surfactant floods, Energy Fuels 26 (2012) 7176–7182, https://doi.org/10.1021/ef301241f.
[21] G. Pérez-Sánchez, J.R.B. Gomes, M. Jorge, Modeling self-assembly of silica/surfactant mesostructures in the templated synthesis of nanoporous solids, Langmuir 29 (2013) 2387–2396, https://doi.org/10.1021/la3046274.
[22] G. Pérez-Sánchez, S.-C. Chien, J.R.B. Gomes, M.N.D.S. Cordeiro, S.M. Auerbach, P. A. Monson, M. Jorge, Multiscale model for the templated synthesis of mesoporous

silica: the essential role of silica oligomers, Chem. Mater. 28 (2016) 2715–2727, https://doi.org/10.1021/acs.chemmater.6b00348.
[23] P. Katiyar, J.K. Singh, A coarse-grain molecular dynamics study of oil–water interfaces in the presence of silica nanoparticles and nonionic surfactants, J. Chem. Phys. 146 (2017), 204702, https://doi.org/10.1063/1.4984073.
[24] E.A. Crespo, J.A.P. Coutinho, A statistical associating fluid theory perspective of the modeling of compounds containing ethylene oxide groups, Ind. Eng. Chem. Res. 58 (2019) 3562–3582, https://doi.org/10.1021/acs.iecr.9b00273.
[25] S. Yada, Y. Yoshioka, M. Ohno, T. Koda, T. Yoshimura, Adsorption and aggregation properties of homogeneous polyoxyethylene alkyl ether- and ester-type nonionic surfactants with multi-branched double chains, Colloids Surf. A: Physicochem. Eng. Asp. 648 (2022), 129247, https://doi.org/10.1016/j.colsurfa.2022.129247.
[26] M.J. Rosen, J.T. Kunjappu, Surfactants and Interfacial Phenomena, John Wiley & Sons, 2012.
[27] A. Léonard, J.L. Blin, B.-L. Su, Synthesis of highly ordered mesoporous compounds with control of morphology using a non-ionic surfactant as template, in: A. Sayari, M. Jaroniec (Eds.), Nanoporous Materials III, Elsevier, 2002, pp. 109–116, https://doi.org/10.1016/S0167-2991(02)80531-6.
[28] K. Holmberg, B. Jönsson, B. Kronberg, B. Lindman. Surfactants and Polymers in Aqueous Solution, 2nd ed., John Wiley & Sons,, Hoboken, NJ, 2003.
[29] S. Garde, L.U. Yang, J.S. Dordick, M.E. Paulaitis, Molecular dynamics simulation of C8E5 micelle in explicit water: structure and hydrophobic solvation thermodynamics, Mol. Phys. 100 (2002) 2299–2306, https://doi.org/10.1080/00268970110118312.
[30] E.A. Crespo, L.F. Vega, G. Pérez-Sánchez, J.A.P. Coutinho, Unveiling the phase behavior of CiEj non-ionic surfactants in water through coarse-grained molecular dynamics simulations, Soft Matter 17 (2021) 5183–5196, https://doi.org/10.1039/D1SM00362C.
[31] J. Eastoe, R.F. Tabor, Surfactants and nanoscience, in: Colloidal Foundations of Nanoscience, Elsevier, 2014, pp. 135–157, https://doi.org/10.1016/B978-0-444-59541-6.00006-0.
[32] J.-H. Ryu, S. Park, B. Kim, A. Klaikherd, T.P. Russell, S. Thayumanavan, Highly ordered gold nanotubes using thiols at a cleavable block copolymer interface, J. Am. Chem. Soc. 131 (2009) 9870–9871, https://doi.org/10.1021/ja902567p.
[33] G.T. Dimitrova, Th.F. Tadros, P.F. Luckham, Investigations of the phase changes of nonionic surfactants using microscopy, differential scanning calorimetry, and rheology. 1. synperonic A7, a C13/C15 Alcohol with 7 mol of ethylene oxide, Langmuir 11 (1995) 1101–1111, https://doi.org/10.1021/la00004a012.
[34] M. Corti, V. Degiorgio, Critical behavior of a micellar solution, Phys. Rev. Lett. 45 (1980) 1045–1048, https://doi.org/10.1103/PhysRevLett.45.1045.
[35] M. Zulauf, J.P. Rosenbusch, Micelle clusters of octylhydroxyoligo(oxyethylenes,), J. Phys. Chem. 87 (1983) 856–862, https://doi.org/10.1021/j100228a032.
[36] D.J. Mitchell, G.J.T. Tiddy, L. Waring, T. Bostock, M.P. McDonald, Phase behaviour of polyoxyethylene surfactants with water. Mesophase structures and partial miscibility (cloud points), J. Chem. Soc., Faraday Trans. 1: Phys. Chem. Condens. Phases 79 (1983) 975–1000, https://doi.org/10.1039/F19837900975.
[37] R. Dong, J. Hao, Complex fluids of poly(oxyethylene) monoalkyl ether nonionic surfactants, Chem. Rev. 110 (2010) 4978–5022, https://doi.org/10.1021/cr9003743.
[38] Y. Nibu, T. Inoue, Phase behavior of aqueous mixtures of some polyethylene glycol decyl ethers revealed by DSC and FT-IR measurements, J. Colloid Interface Sci. 205 (1998) 305–315, https://doi.org/10.1006/jcis.1998.5621.
[39] J.C. Lang, R.D. Morgan, Nonionic surfactant mixtures. I. Phase equilibria in C10E4–H2O and closed-loop coexistence, J. Chem. Phys. 73 (1980) 5849–5861, https://doi.org/10.1063/1.440028.
[40] B.A. Mulley, A.D. Metcalf, Nonionic surface-active agents. Part VI. Phase equilibria in binary and ternary systems containing nonionic surface-active agents, J. Colloid Sci. 19 (1964) 501–515, https://doi.org/10.1016/0095-8522(64)90066-2.
[41] J.S. Clunie, J.M. Corkill, J.F. Goodman, P.C. Symons, J.R. Tate, Thermodynamics of non-ionic surface-active agent + water systems, Trans. Faraday Soc. 63 (1967) 2839–2845, https://doi.org/10.1039/TF9676302839.
[42] S.S. Funari, G. Rapp, X-ray Studies on the C12EO2/Water System, J. Phys. Chem. B 101 (1997) 732–739, https://doi.org/10.1021/jp9629250.
[43] M.L. Lynch, K.A. Kochvar, J.L. Burns, R.G. Laughlin, Aqueous-Phase Behavior and Cubic Phase-Containing Emulsions in the C12E2−Water System, Langmuir 16 (2000) 3537–3542, https://doi.org/10.1021/la991366w.
[44] J.S. Clunie, J.F. Goodman, P.C. Symons, Phase equilibria of dodecylhexaoxyethylene glycol monoether in water, Trans. Faraday Soc. 65 (1969) 287–296, https://doi.org/10.1039/TF9696500287.
[45] K. Shinoda, Thermodynamic aspects of nonionic surfactant—water systems, J. Colloid Interface Sci. 34 (1970) 278–282, https://doi.org/10.1016/0021-9797(70)90179-7.
[46] V. Degiorgio, R. Piazza, M. Corti, C. Minero, Critical properties of nonionic micellar solutions, J. Chem. Phys. 82 (1985) 1025–1031, https://doi.org/10.1063/1.448570.
[47] E. Jahns, H. Finkelmann, Lyotropic liquid crystalline phase behavior of a polymeric amphiphile polymerized via their hydrophilic ends, Colloid Polym. Sci. 265 (1987) 304–311, https://doi.org/10.1007/BF01417929.
[48] F. Sterpone, G. Briganti, C. Pierleoni, Molecular dynamics study of spherical aggregates of chain molecules at different degrees of hydrophilicity in water solution, Langmuir 17 (2001) 5103–5110, https://doi.org/10.1021/la000750m.
[49] F. Sterpone, C. Pierleoni, G. Briganti, M. Marchi, Molecular dynamics study of temperature dehydration of a C12E6 spherical micelle, Langmuir 20 (2004) 4311–4314, https://doi.org/10.1021/la035964t.
[50] T.M. Ferreira, D. Topgaard, O.H.S. Ollila, Molecular conformation and bilayer pores in a nonionic surfactant lamellar phase studied with 1H–13C solid-state NMR and molecular dynamics simulations, Langmuir 30 (2014) 461–469, https://doi.org/10.1021/la404684r.
[51] C. Senac, W. Urbach, E. Kurtisovski, P.H. Hünenberger, B.A.C. Horta, N. Taulier, P. F.J. Fuchs, Simulating bilayers of nonionic surfactants with the GROMOS-compatible 2016H66 force field, Langmuir 33 (2017) 10225–10238, https://doi.org/10.1021/acs.langmuir.7b01348.
[52] H. Lee, R.M. Venable, A.D. MacKerell, R.W. Pastor, Molecular dynamics studies of polyethylene oxide and polyethylene glycol: hydrodynamic radius and shape anisotropy, Biophys. J. 95 (2008) 1590–1599, https://doi.org/10.1529/biophysj.108.133025.
[53] D. Ji, G. Liu, X. Zhang, C. Zhang, S. Yuan, Molecular dynamics study on the adsorption of heavy oil drops on a silica surface with different hydrophobicity, Energy Fuels 34 (2020) 7019–7028, https://doi.org/10.1021/acs.energyfuels.0c00996.
[54] H. Zhang, Y. Ma, Q. Hao, H. Wang, G. Liu, S. Yuan, Molecular dynamics study on mechanism of preformed particle gel transporting through nanopores: surface hydration, RSC Adv. 6 (2016) 7172–7180, https://doi.org/10.1039/C5RA24282G.
[55] S.J. Marrink, H.J. Risselada, S. Yefimov, D.P. Tieleman, A.H. de Vries, The MARTINI force field: coarse grained model for biomolecular simulations, J. Phys. Chem. B 111 (2007) 7812–7824, https://doi.org/10.1021/jp071097f.
[56] W. Shinoda, R. DeVane, M.L. Klein, Multi-property fitting and parameterization of a coarse grained model for aqueous surfactants, Mol. Simul. 33 (2007) 27–36, https://doi.org/10.1080/08927020601054050.
[57] W. Shinoda, R. DeVane, M.L. Klein, Coarse-grained molecular modeling of non-ionic surfactant self-assembly, Soft Matter 4 (2008) 2454–2462, https://doi.org/10.1039/B808701F.
[58] S.A. Sanders, A.Z. Panagiotopoulos, Micellization behavior of coarse grained surfactant models, J. Chem. Phys. 132 (2010), 114902, https://doi.org/10.1063/1.3358354.
[59] M. Velinova, D. Sengupta, A.V. Tadjer, S.-J. Marrink, Sphere-to-rod transitions of nonionic surfactant micelles in aqueous solution modeled by molecular dynamics simulations, Langmuir 27 (2011) 14071–14077, https://doi.org/10.1021/la203055t.
[60] M. Velinova, Y. Tsoneva, A. Ivanova, A. Tadjer, Estimation of the mutual orientation and intermolecular interaction of C12Ex from molecular dynamics simulations, J. Phys. Chem. B 116 (2012) 4879–4888, https://doi.org/10.1021/jp212047r.
[61] G. Rossi, P.F.J. Fuchs, J. Barnoud, L. Monticelli, A coarse-grained MARTINI model of polyethylene glycol and of polyoxyethylene alkyl ether surfactants, J. Phys. Chem. B 116 (2012) 14353–14362, https://doi.org/10.1021/jp3095165.
[62] M. Vuorte, J. Määttä, M. Sammalkorpi, Simulations study of single-component and mixed n-Alkyl-PEG micelles, J. Phys. Chem. B. 122 (2018) 4851–4860, https://doi.org/10.1021/acs.jpcb.8b00398.
[63] T. Taddese, P. Carbone, Effect of chain length on the partition properties of poly (ethylene oxide): comparison between MARTINI coarse-grained and atomistic models, J. Phys. Chem. B 121 (2017) 1601–1609, https://doi.org/10.1021/acs.jpcb.6b10858.
[64] R. Alessandri, F. Grünewald, S.J. Marrink, The martini model in materials science, Adv. Mater. 33 (2021) 2008635, https://doi.org/10.1002/adma.202008635.
[65] F. Grunewald, G. Rossi, A.H. de Vries, S.J. Marrink, L. Monticelli, Transferable MARTINI model of poly(ethylene oxide), J. Phys. Chem. B 122 (2018) 7436–7449, https://doi.org/10.1021/acs.jpcb.8b04760.
[66] S.C. Chien, G. Pérez-Sánchez, J.R.B. Gomes, M.N.D.S. Cordeiro, M. Jorge, S. M. Auerbach, P.A. Monson, Molecular simulations of the synthesis of periodic mesoporous silica phases at high surfactant concentrations, J. Phys. Chem. C. 121 (2017) 4564–4575, https://doi.org/10.1021/acs.jpcc.6b09429.
[67] P.C.T. Souza, R. Alessandri, J. Barnoud, S. Thallmair, I. Faustino, F. Grünewald, I. Patmanidis, H. Abdizadeh, B.M.H. Bruininks, T.A. Wassenaar, P.C. Kroon, J. Melcr, V. Nieto, V. Corradi, H.M. Khan, J. Domański, M. Javanainen, H. Martinez-Seara, N. Reuter, R.B. Best, I. Vattulainen, L. Monticelli, X. Periole, D. P. Tieleman, A.H. de Vries, S.J. Marrink, Martini 3: a general purpose force field for coarse-grained molecular dynamics, Nat. Methods 18 (2021) 382–388, https://doi.org/10.1038/s41592-021-01098-3.
[68] M. Abraham, T. Murtola, R. Schulz, S. Páll, J. Smith, B. Hess, E. Lindahl, GROMACS: High performance molecular simulations through multi-level parallelism from laptops to supercomputers, SoftwareX 1 (2015), https://doi.org/10.1016/j.softx.2015.06.001.
[69] R.W. Hockney, S.P. Goel, J.W. Eastwood, Quiet high-resolution computer models of a plasma, J. Comput. Phys. 14 (1974) 148–158, https://doi.org/10.1016/0021-9991(74)90010-2.
[70] T. Darden, D. York, L. Pedersen, Particle mesh Ewald: An N·log(N) method for Ewald sums in large systems, J. Chem. Phys. 98 (1993) 10089–10092, https://doi.org/10.1063/1.464397.
[71] G. Bussi, D. Donadio, M. Parrinello, Canonical sampling through velocity rescaling, J. Chem. Phys. 126 (2007), 014101, https://doi.org/10.1063/1.2408420.
[72] B. Hess, H. Bekker, H.J.C. Berendsen, J.G.E.M. Fraaije, LINCS: A linear constraint solver for molecular simulations, J. Comput. Chem. 18 (1997) 1463–1472, https://doi.org/10.1002/(SICI)1096-987X(199709)18:12<1463::AID-JCC4>3.0.CO;2-H.
[73] M. Bulacu, N. Goga, W. Zhao, G. Rossi, L. Monticelli, X. Periole, D.P. Tieleman, S. J. Marrink, Improved angle potentials for coarse-grained molecular dynamics simulations, J. Chem. Theory Comput. 9 (2013) 3282–3292, https://doi.org/10.1021/ct400219n.
[74] E. Perrin, M. Schoen, F.-X. Coudert, A. Boutin, Structure and dynamics of solvated polymers near a silica surface: on the different roles played by solvent, J. Phys. Chem. B 122 (2018) 4573–4582, https://doi.org/10.1021/acs.jpcb.7b11753.

[75] L. Martínez, R. Andrade, E.G. Birgin, J.M. Martínez, PACKMOL: A package for building initial configurations for molecular dynamics simulations, J. Comput. Chem. 30 (2009) 2157–2164, https://doi.org/10.1002/jcc.21224.
[76] W. Humphrey, A. Dalke, K. Schulten, VMD: Visual molecular dynamics, J. Mol. Graph 14 (1996) 33–38, https://doi.org/10.1016/0263-7855(96)00018-5.
[77] J. Hoshen, R. Kopelman, Percolation and cluster distribution. I. Cluster multiple labeling technique and critical concentration algorithm, Phys. Rev. B. 14 (1976) 3438–3445, https://doi.org/10.1103/PhysRevB.14.3438.
[78] J.M. Corkill, J.F. Goodman, R.H. Ottewill, Micellization of homogeneous non-ionic detergents, Trans. Faraday Soc. 57 (1961) 1627–1636, https://doi.org/10.1039/TF9615701627.
[79] J.S. Marland, B.A. Mulley, Effect of micelle formation and the nature of the oil-phase on the distribution of a non-ionic surfactant in three- and four-component emulsions, J. Pharm. Pharmacol. 24 (1972) 729–734, https://doi.org/10.1111/j.2042-7158.1972.tb09098.x.
[80] G. Stangl, R. Niessner, Cloud point extraction of napropamide and thiabendazole from water and soil, Microchim. Acta 113 (1994) 1–8, https://doi.org/10.1007/BF01243131.
[81] P. Levitz, Aggregative adsorption of nonionic surfactants onto hydrophilic solid/water interface, Relat. Bulk. micellization, Langmuir 7 (1991) 1595–1608, https://doi.org/10.1021/la00056a010.
[82] S.E. Anachkov, K.D. Danov, E.S. Basheva, P.A. Kralchevsky, K. P. Ananthapadmanabhan, Determination of the aggregation number and charge of ionic surfactant micelles from the stepwise thinning of foam films, Adv. Colloid Interface Sci. 183– 184 (2012) 55–67, https://doi.org/10.1016/j.cis.2012.08.003.
[83] W.C. Griffin, Calculation of HLB values of non-ionic surfactants, J. Soc. Cosmet. Chem. 5 (1954) 249–256.
[84] D.B. Miraglia, J.L. Rodríguez, R.M. Minardi, P.C. Schulz, Critical micelle concentration and HLB of the sodium oleate–hexadecyltrimethylammonium bromide mixed system, J. Surfactants Deterg. 14 (2011) 401–408, https://doi.org/10.1007/s11743-010-1239-y.